Full Length Article

Generation of 2D-arrays of anisotropically shaped nanoparticles by nanosecond laser-induced periodic surface patterning

Sebastian Durbach, Norbert Hampp[*]

University of Marburg, Department of Chemistry, Hans-Meerwein Str. 4, 35032 Marburg, Germany

ARTICLE INFO

ABSTRACT

Two-dimensional surface pattern formation is achieved by irradiation of a gold thin film on a silicon wafer by circular- or non-polarized nanosecond laser pulses. It is shown that the laser-induced reorganization may be described by the same principles as laser-induced periodic surface structure (LIPPS) formation using linear polarized light, which generates typical stripe-like patterns. The 2D-process shows some astonishing similarities with a simple interference feedback loop modeling material redeposition. The periodicity Λ of the created hexagonal and square patterns is in good agreement with calculations of the theoretically calculated wavelength of surface plasmon polaritons (SPPs). The morphology of the created nanoparticles is analyzed with focused ion beam scanning electron microscopy (FIB-SEM), revealing the dependence on the substrate's crystallographic orientation. Generated patterns may be either converted into 'nanohole' arrays or used for the synthesis of exotically shaped and highly uniform gold nanoparticles.

1. Introduction

In recent years, the fabrication of micro- and nanostructures with specific spatial arrangements has attracted ever-growing attention, as it enables the control of substrates physio-chemical properties. By their various properties and quantum behavior, these functionalized surfaces are utilized in a vast range of different applications including solar cells [1], decorations [2], superhydrophobicity [3], biosensing [4,5], bio-mimetic [6], electronics [7] and photonic applications [8]. As lithographic or multi-beam [9,10] techniques are either time consuming and/or require rather complex and costly equipment, laser-induced self-organizing patterning is a promising alternative for extended surface areas [11].

For nanosecond laser pulses typically low spatial frequency LIPSS (LSFL), further on referred to as 1D-LIPSS, with spatial periodicities similar to the applied laser wavelength are obtained, which are known since their first discovery by Birnbaum in 1965 [12]. The underlying formation mechanism of LIPSS is still highly debated [13–18]. Nevertheless it is commonly accepted, that interference of the incident light and surface plasmon polaritons (SPP), arising from the substrates'

surface roughness, leads to periodic modulations of absorbed energy [13–16,19,20]. The corresponding inhomogeneous energy distributions give rise to thermal gradients resulting in cumulative hydrodynamic effects like thermocapillary forces, which are known to be an essential force driving the liquid flow in ns-laser melted metal thin films [21]. Advanced numerical simulations, often based on the Sipe-Drude-model, and taking into account optical and thermal substrate properties within an inter- and intra-pulse feedback mechanism, are in good agreement with experimental 1D-LIPSS features [22–25]. Pulse fluence, pulse number, and geometric pulse overlap are key parameters for tuning the structure's features [16,19,26,27].

Even though 1D-LIPSS has been a scientific evergreen in the past few decades, the fabrication of 2D-LIPSS only recently gained some popularity. 2D-LIPSS are either generated by irradiation of two crossed linear-polarized consecutive pulses [28–31] or by use of circularly polarized pulses [28,29,32,33].

In this article, we demonstrate the laser-induced self-organization of a gold thin film on silicon wafers of different crystallographic orientations, treated with nanosecond laser pulses. This model system is well characterized for one-dimensional nanostructure fabrication as shown

---

* Corresponding author.
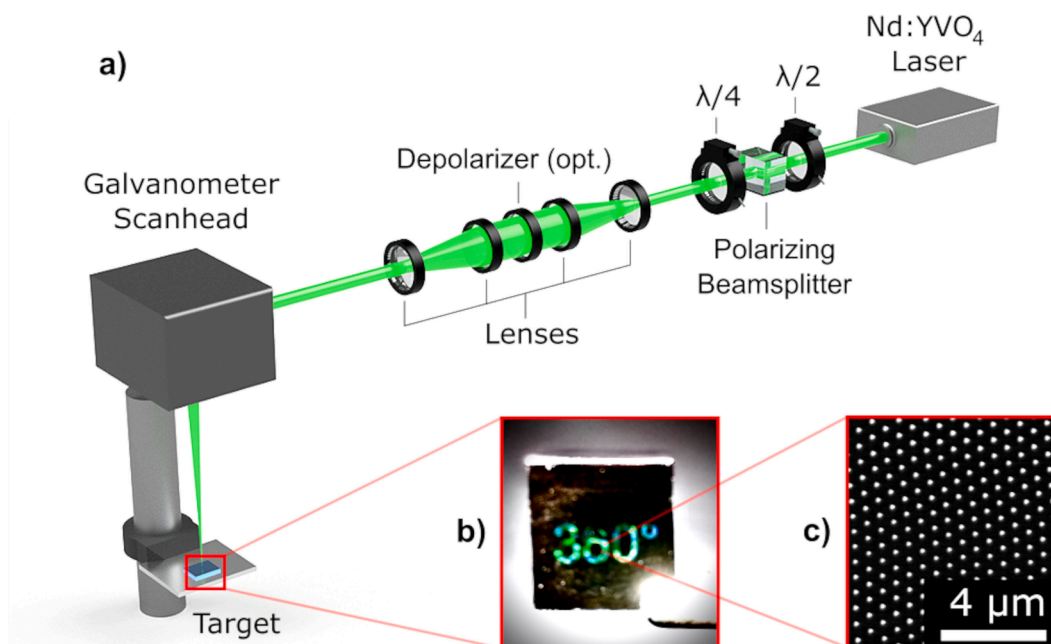*E-mail addresses:* durbachs@staff.uni-marburg.de (S. Durbach), hampp@uni-marburg.de (N. Hampp).

Fig. 1. a) Laser setup able to control ellipticity and degree of polarization. λ/2 and λ/4: half-wave and quarter-wave plates. b) Photo of wafer fragment featuring white light diffraction of AuSi-2D-LIPSS. c) SEM image of AuSi pattern formed by 2D-LIPSS process.

in previous work [34]. Under irradiation with both, circular and depolarized light, two-dimensional nanoparticle arrays emerge, providing a highly symmetric pattern.

2. Materials and methods

2.1. Experimental

The silicon samples used in this study were mechano-chemically polished boron-doped $(1\,0\,0)$ (Siegert Wafer, Germany) and $(1\,1\,1)$ (Silchem, Germany) single crystals. The wafers were gold coated with 1.8–4.6 nm gold using an Auto 206 vacuum coater system (Edwards, U. K.). The thickness of the generated Au thin film was measured with single-wavelength ellipsometry. Laser irradiation was performed with a frequency-doubled Nd:YVO$_4$ diode-pumped solid-state (DPSS) laser (explorer XP 532-5, Newport, USA) emitting ≈ 8 ns pulses (FWHM) of $\lambda_0 = 532$ nm wavelength in TEM$_{00}$ ($M^2 < 1.1$) mode. The ns-laser pulses were focused to a spot radius of 50 μm ($1/e^2$) at normal incidence to the substrate surface. The beam was scanned over the substrate by a galvanometer scan head (SCANgine 14-532, Scanlab, Germany). The polarization state of the laser was measured with a polarimeter (Thorlabs TXP 5004 with the PAN5710VIS scan head). The laser power was measured with an LM-80 V detector head (FieldMax II, Coherent USA).

Scanning electron microscopy (SEM) was performed on a field emission microscope (JSM-7500F, Jeol, Japan) equipped with a backscattered electron detector (YAG, Autrata, Czech Republic) and with focussed ion beam milling (FIB) on a CrossBeam-Workstation (Gemini 2, Carl Zeiss, Germany).

Generated gold nanoparticles can be harvested by a simple two-step etching process, first with 1 M fluoric acid (HF), and second with a boiling 4:1 mixture of concentrated KOH$_{aq.}$ and 2-propanol.

The surface topography of 2D-LIPSS substrates after acid-etching (HF (1 M), aqua regia) was analyzed by atomic force microscopy (AFM, Nanoscope IV, Bruker, USA). Taping mode was chosen for topological imaging using SNL-10 tips (f = 56 kHz).

2.2. Image processing

Gwyddion, an open-source software, was used for the analysis of the local pattern symmetry and spatial frequency, and 2D-Fast-Fourier-Transformation (FFT) of the SEM images.

3. Theory

Previous studies suggest that LIPSS are created by incident wavefronts interfering with SPP [13–16,19,20]. SPP describe charge density oscillations propagating along with the interface of a dielectric and a conducting substrate with a specific wavelength λ_{SPP} [35]. This approach represents a useful explanation of LIPSS formation on metals and semiconductors as SPP are transverse magnetically polarized in relation to the laser light polarization [36]. SPP may be excited through diffraction of light at surface irregularities if an optically active mode near the laser frequency exists. The wavelength λ_{SPP} is shorter than the laser wavelength as can be derived from Eq. (1) [35],

$$\lambda_{SPP} = \lambda_0 \sqrt{\frac{\varepsilon_S' + \varepsilon_d}{\varepsilon_S' \cdot \varepsilon_d}} \tag{1}$$

where ε_S' is the real part of the metallic substrates dielectric function and ε_d the dielectric function of the dielectric layer. Using the complex dielectric function the penetration depth and propagation length can be calculated as shown in Appendix A. Neglecting the thin gold layer the dielectric function of the dielectric can be considered to be the dielectric function of air $\varepsilon_{d(Air)} = 1$ [37]. Assuming the massive excitation and heating, e.g. liquefaction of the silicon at the air/Si interface, the dielectric function of the substrate equals the optical properties of molten silicon with $\varepsilon_{S(mSi)}^{Å} = -14.2$ [38]. This has proven to be a good assumption in earlier works [20] and predicts a theoretical wavelength of $\lambda_{SPP} = 513$ nm which is in good agreement with the measured periodicity ($\Lambda = 515$ nm $\pm$ 13 nm) of our 2D-LIPSS (see Fig. 1).

3.1. Results and discussion

3.1.1. Pattern formation

LIPSS were generated on Si$(1\,0\,0)$-wafers covered with a 3.4 nm Au thin film. Different states of ellipticity of the laser polarization were employed. The generated LIPSS is oriented perpendicular to the main
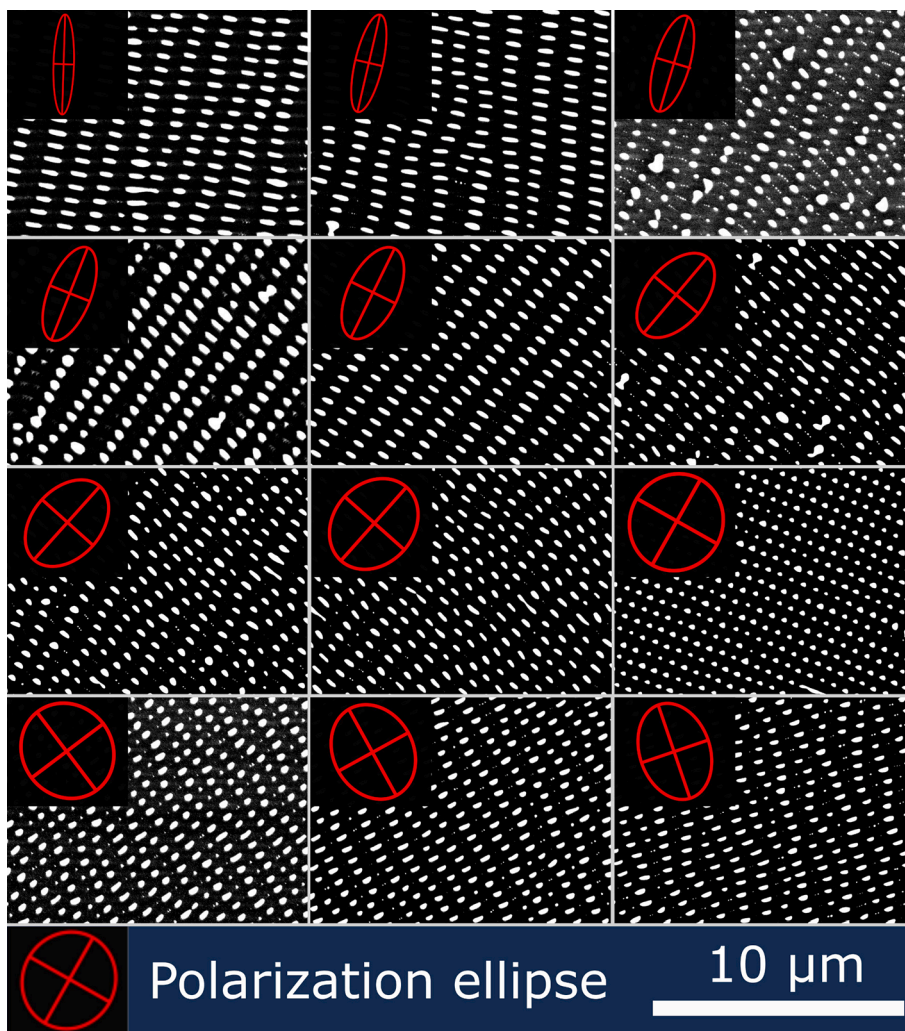
Fig. 2. LIPSS on Si(1 0 0) coated with Au ($d = 3.4$ nm) after irradiation ($F_p = 0.145$ J/cm^2 , N = 753) with different polarization states from nearly linear to circular polarization. The polarization ellipse of the incident laser radiation (red) indicates the polarization used for each corresponding particle pattern.
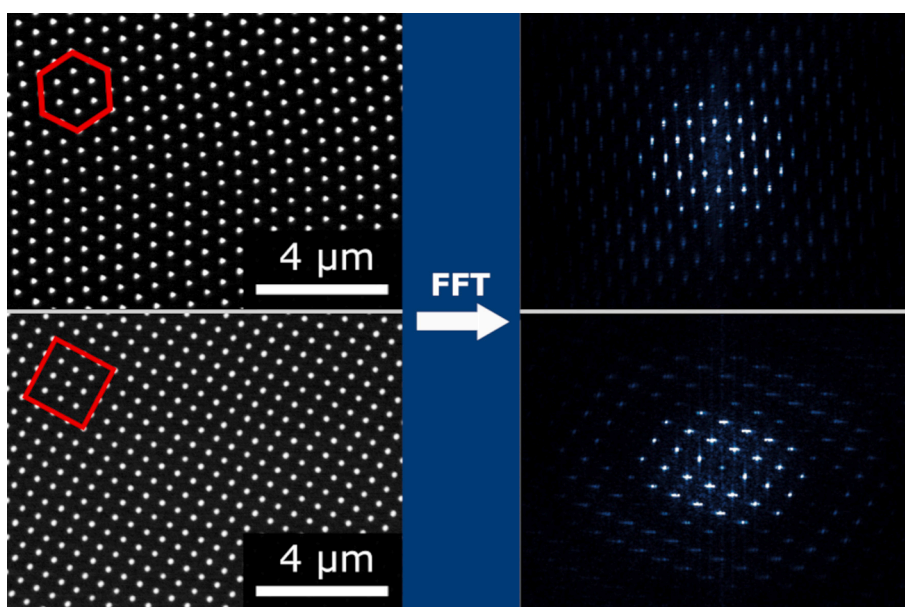

Fig. 3. 2D-LIPSS generated by irradiation with circularly polarized light on Si(1 0 0) with hexagonal (a) (d = 4.1 nm, $F_p = 0.155$ J/cm^2 , N = 5000) and square (b) (d = 2.6 nm , $F_p = 0.152$ J/cm^2 , N = 1500) pattern. c,d) show the Fast Fourier Transformation of the corresponding SEM images.
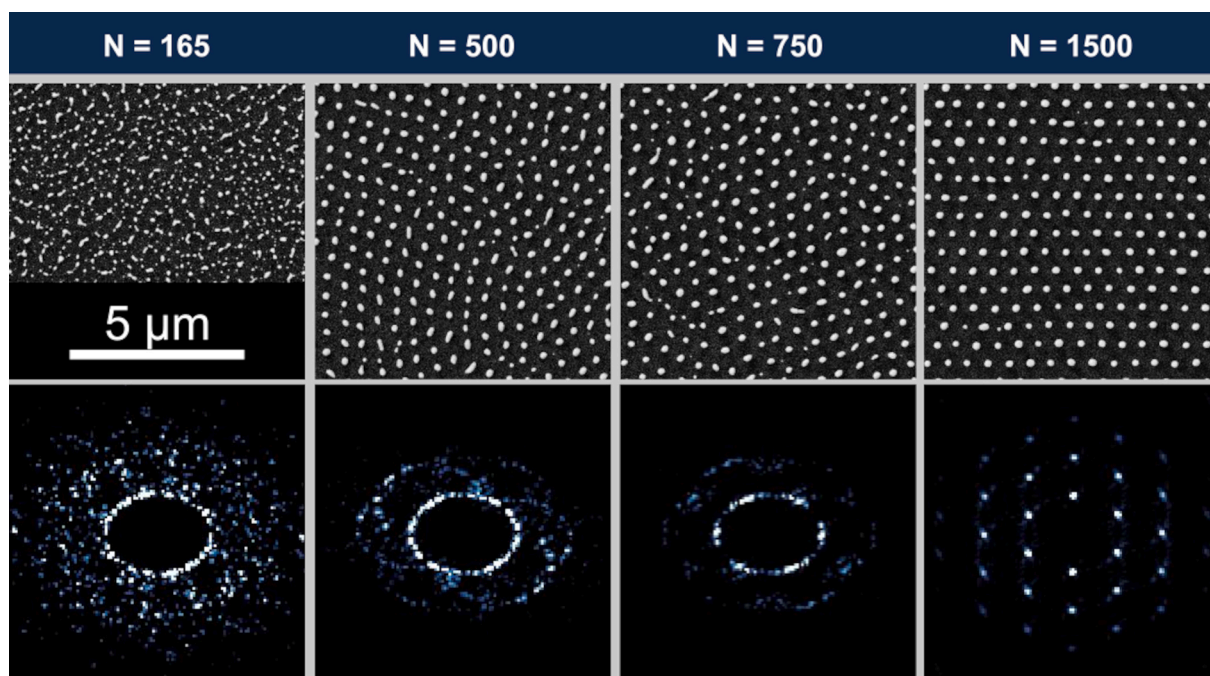
Fig. 4. 2D-LIPSS pattern evolution in relation to the number of laser pulses N with circularly polarized light. (FFT below) (d = 3.6 nm, F_p = 0.125 J/cm^2).

axis of polarization but is disintegrated into droplets for elliptically polarized light (Fig. 2). This disintegration is known to occur upon excessive laser stimulation [17] and is because all LIPSS from Fig. 2 were generated with the same pulse fluence F_p and effective pulse numbers N, which was chosen to fit best for the generation of 2D-LIPSS. 2D-LIPSS were only observed for a polarization ellipticity of 42 deg. or higher, whereby 45 deg. corresponds to circular polarization. The 2D patterns obtained from patterning with circularly polarized light possess either a four- or sixfold symmetry (Fig. 3) as discussed later in this work.

Starting with the very first laser pulse [39,40] the spatial redistribution of the gold thin film begins driven by the intensity pattern formed by the scattered laser light and the SPP at the interface between the semiconducting substrate and the air. Note that the properties of the substrate change during laser irradiation, as further elaborated in

section three (Theory). Typically the dewetting process is driven by melt instabilities against capillary waves induced by small irregularities in the gold layer and results in a spinodal decomposition of the film. The resulting wavelength has a quadratic dependency on the film thickness d [21,41–45].

Despite resembling a typical spinodal decomposition, the power spectra of the dewetted gold films (Fig. 4.) present a wavelength of 515 nm and lack any correlation with the thin film thickness, indicating that the dewetting process is not driven by a homogenous energy absorption of the thin film, but by the substrate's photonic properties. This spatial distribution can be explained by the stimulation of SPPs. As described by Sipe et al. [46], the existence of small irregularities on a surface leads to polarization-dependent scattering and thus energy variations in the surface of the material. For circular polarization, the corresponding
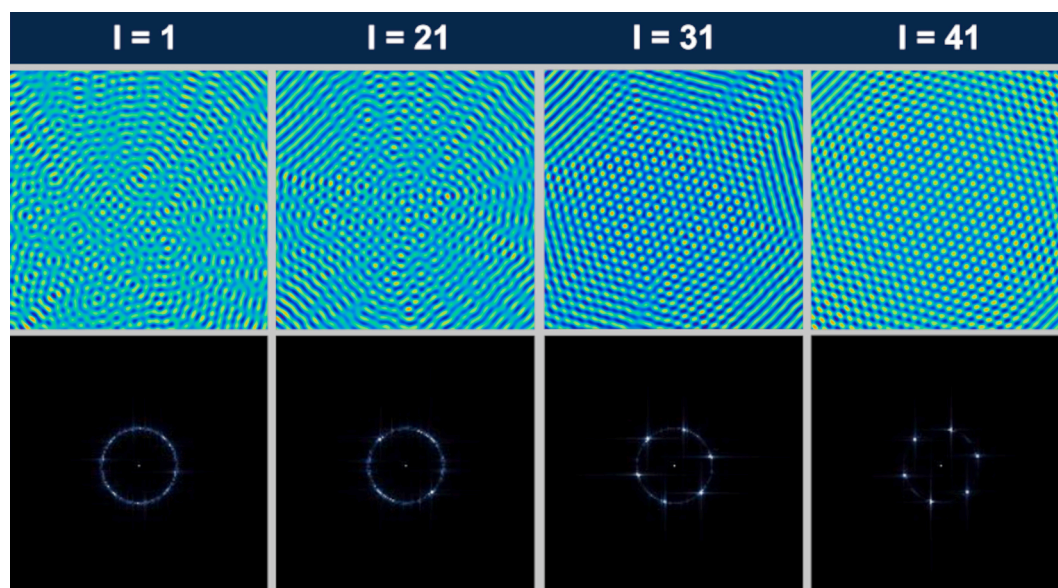

Fig. 5. Interference patterns generated through feedback loop after I iterations. Scattering centers are generated from each previous iteration. (Bottom row) Corresponding FFT frequency patterns.
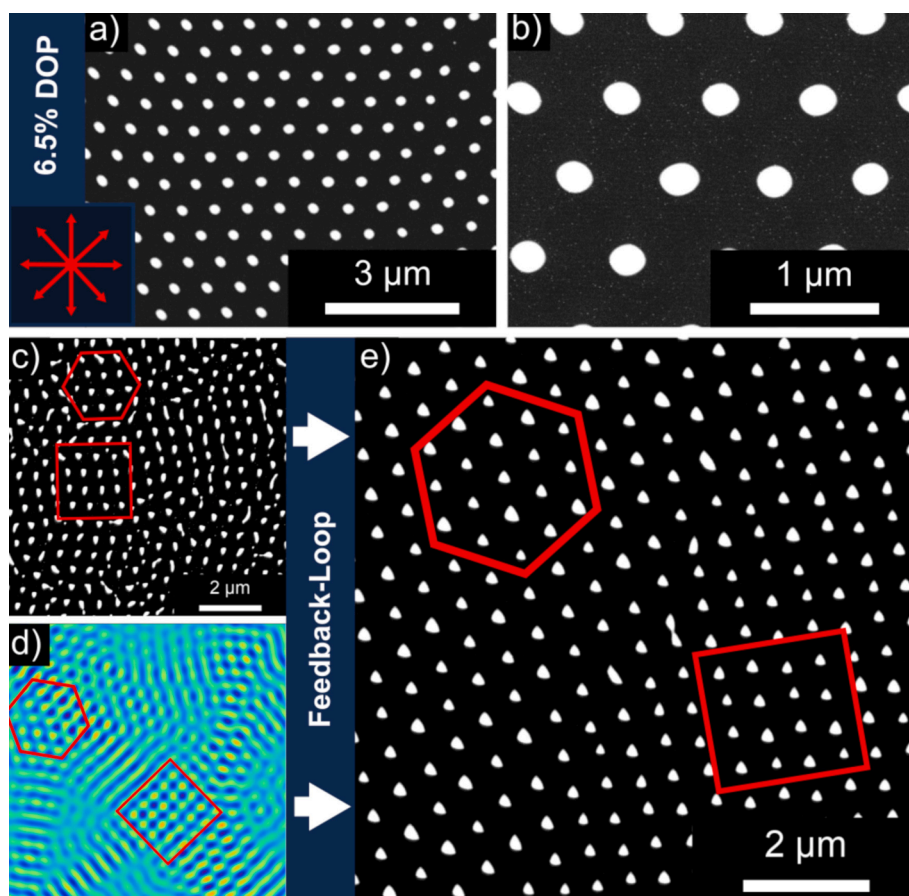
Fig. 6. (a, b) Hexagonal 2D-LIPSS generated with non-polarized light (6.5% DOP). (d = 3.3 nm, F_p = 0.181 J/cm^2 , N = 2475). (c) 2D-LIPSS in an early formation stage showing small domains of nano-particles with hexagonal or square arrangements in immediate proximity (d = 3.8 nm, F_p = 0.145 J/cm^2 , N = 215). (d) Simulated interference patterns (I = 29) showing small domains of hexagonal and square patterns in immediate proximity. (e) 2D-LIPSS showing the interface between an extended domain of square and hexagonal patterns. (d = 2.2 nm, F_p = 0.125 J/cm^2 , N = 1500).

diffraction pattern shows a uniformly bright circle, which is in good agreement with the observed power spectrum of an early stage of pattern formation (Fig. 4). The same graphical illustration of square pattern formation can be found in Appendix A Fig. A1 [47].

Repeated laser stimulation leads to continuous structure refinement and eventually results in nanoparticle arrays with a periodicity of about 515 nm. Note that the nearest neighbor distance of the hexagonally arranged nanoparticles is larger than the corresponding distance in the square pattern, as it follows from geometrical considerations (Fig. A2). During this process, the radial symmetry of the diffraction pattern enhances into six respectively four dominating spatial directions corresponding to hexagonal or square pattern formation. As the equilibrium dewetting time and the temporal spacing of the pulses (10 μs) are much larger than the time where 'molten' gold is existing during the laser pulse duration of a few nanoseconds, the SEM images after a defined number of pulses N correspond to a time-series of snapshots of the pattern formation, based on rapid resolidification detaining the fluid morphology [43].

Unlike experiments with linear polarization, no inherent component favoring a certain alignment of the nanostructures was observed. To investigate the underlying mechanism of pattern formation we used a simplistic simulation demonstrating a positive feedback loop capable of evolving regular patterns from chaotic wave interactions. The feedback loop evolves from an initial set of randomly distributed scattering sources. Each iteration calculates the interference pattern of all scattering sources created by the previous iterations topographic modulation. A detailed explanation of the simulation procedure may be found in Appendix B.

Fig. 5 illustrates the interference patterns after "I" iterations which reflects the number N of effective pulses. Despite the simplicity of the simulated interference patterns, the pattern evolution shows striking similarity with the formation evolution of 2D-LIPSS. After an initial random spatial distribution with radial symmetry (single wavelength), local well-arranged patterns emerge. This emerging local pattern dominates the neighboring superposition of scattered waves which leads to the proliferation of the very same pattern after further iterations. This development is seen in both the experimental results and the interference simulation. (Fig. 4. and Fig. 5).

As a consequence of this model for the pattern formation, there is no need for circular polarization for a 2D-LIPSS generation as long as the system has no predominant direction component. This assumption proves to be well-founded as we generated hexagonal 2D-LIPSS with depolarized light using a depolarizer (Fig. 6).

The probability for the nanoparticles to locally align in both, square and hexagonal seed patterns, (Fig. 6 c,d), results in the presence of both symmetries in immediate proximity (Fig. 6 e) or the coexistence of two independent patterns possessing the same symmetry but different orientations. An illuminated area consists of different domains that have been found to range from 100 μm^2 up to several tens of mm^2. Fig. 7 recapitulates the pattern formation and schematically illustrates the synchronous existence of different patterns on extended irradiated areas. The patches can be macroscopically revealed with white light diffraction under different angles, as only areas with patterns matching the angle of incidence show diffraction. Öktem et al. [48] obtained comparable results by linking quality control issues for many feedback-driven lasers fabricated nanostructures to the dimension of the laser spot radius, as a larger radius allows the concurrent formation of multiple seed locations bearing the blame of pattern irregularities.

As demonstrated random pattern formation on a small scale and subsequent proliferation through self-similarity can result in different pattern symmetries despite being exposed to the same laser stimulus. Theoretical studies have shown, that only 4-fold and 6-fold symmetries
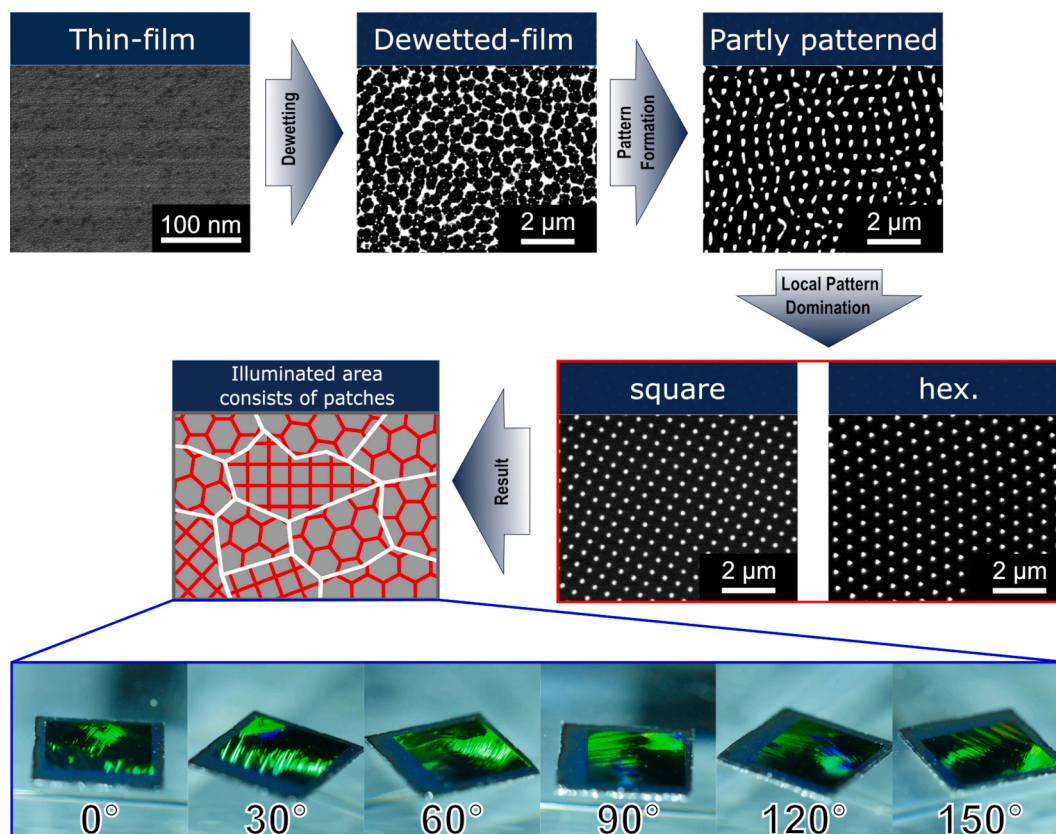
Fig. 7. Schematic representation of the pattern evolution in different domains upon recurrent laser stimulation with circularly polarized light. Bellow: White light diffraction of a 1×1 cm 2D-LIPSS area under different angles of illumination.

occur in such types of systems, which is exactly what we found in our AuSi-system [49,50]. Therefore we investigated the probability of both, hexagonal and square nano-dot arrangements. Despite the Si(1 0 0) showing a marginal higher tendency for the formation of hexagonal patterns, both Si(1 0 0)-wafers and Si(1 1 1)-wafer show an increasing probability for hexagonal pattern formation upon high effective pulse numbers N, as generally preferred in similar, dynamic systems [25] (Fig. 8 a,b). For fewer effective pulse numbers N, an increased occurrence of square patterns with higher pulse fluence is observed. This is in good agreement with recent observations attributing the symmetry shift of 2D-LIPSS to changes in convection flows related to spatial and temporal energy dose distributions [28,31]. As a consequence there is a change in temperature gradients and thus a change in viscosity of the melted material. This affects the so-called Prandtl-number, a dimensionless number defining the ratio of momentum diffusivity to thermal diffusivity, which is well known as a key component for pattern selection in convection systems [25,51,52].

Another important pattern selection mechanism can be attributed to surface defects which are expected in highly dynamic environments generated through ns-laser irradiation. To generate linear surface modifications serving as model-defects, a Si(1 0 0)-wafer was irradiated by a UV-laser (355 nm) previous to proceeding with the usual procedure for a 2D-LIPSS generation (Fig. 8 c). At the interface between the untreated and the pre-irradiated area, a significant deviation of the nano-dot structures' main axis occurs (Fig. 8 d) even if no apparent surface damage could be observed beforehand. This demonstrates the effect of statistically occurring surface defects on preferred pattern formation.

No other variable, neither the thickness of the Au thin film (1.2–5 nm) nor the hatch rotation and distance, which could account for the pattern formation boundary conditions, could be identified to influence the pattern selection. The shallow modulation depth (d < 10 nm) further reinforces the suggested formation mechanism involving melting,

material displacement, and resolidification, rather than an ablative mechanism [53]. To further investigate the exact interaction and weighting of hydrodynamic versus photonic effects during 2D-LIPSS formation upon ns-laser irradiation of metal thin films, sophisticated numerical simulations taking into account inhomogeneous energy absorbance, electromagnetic scattering, thermal effects, and material flow need to be developed which is out of the scope of the present work.

3.2. Goldparticle properties

The properties of nanoparticle arrays are not solely defined by their order but are also influenced by the features of their individual elements. Particles fabricated on Si(1 0 0)- and Si(1 1 1)-interfaces were analyzed via focussed ion beam (FIB) milling and reconstructed via serial section imaging (SSI). The 3D-morphology of the nanoparticles generated on the Si(1 0 0)-surface resembles the shape of lentils (Fig. 9 a), whereas the nanoparticles generated on the Si(1 0 1 0 1)-surface possess the shape of bulged triangles (Fig. 9 e).

The gold nanoparticles are partly sunken into the surface as can be seen in their respective cross-section (Fig. 9 b,f), similar as reported for gold nanowires fabricated by a similar Au/Si system by Reinhardt et al. [34]. Reinhardt et al. performed a composition study (EDX) on a cross sections of their ns-pulsed laser generated nanowires and report a significant amount of Si, in particular in the outer region of the nano-structures. XRD experiments showed a small shoulder at $2\theta = 39.7°$, corresponding to the $(I4\overline{3}m)$ Au/Si eutectic phase, further underlining the presence of a small amount of Au/Si-alloy and strongly suggesting a similar alloying process in the peripheral region of gold nanoparticles generated in this work. The lenticular shape of the particles generated on a Si(1 0 0)-surface (Fig. 9 b) is expected for nearly isotropic dewetting with high interfacial energy [54,55]. Gold nanoparticles generated on a Si(1 1 1)-surface on the other hand show significant deviance of the
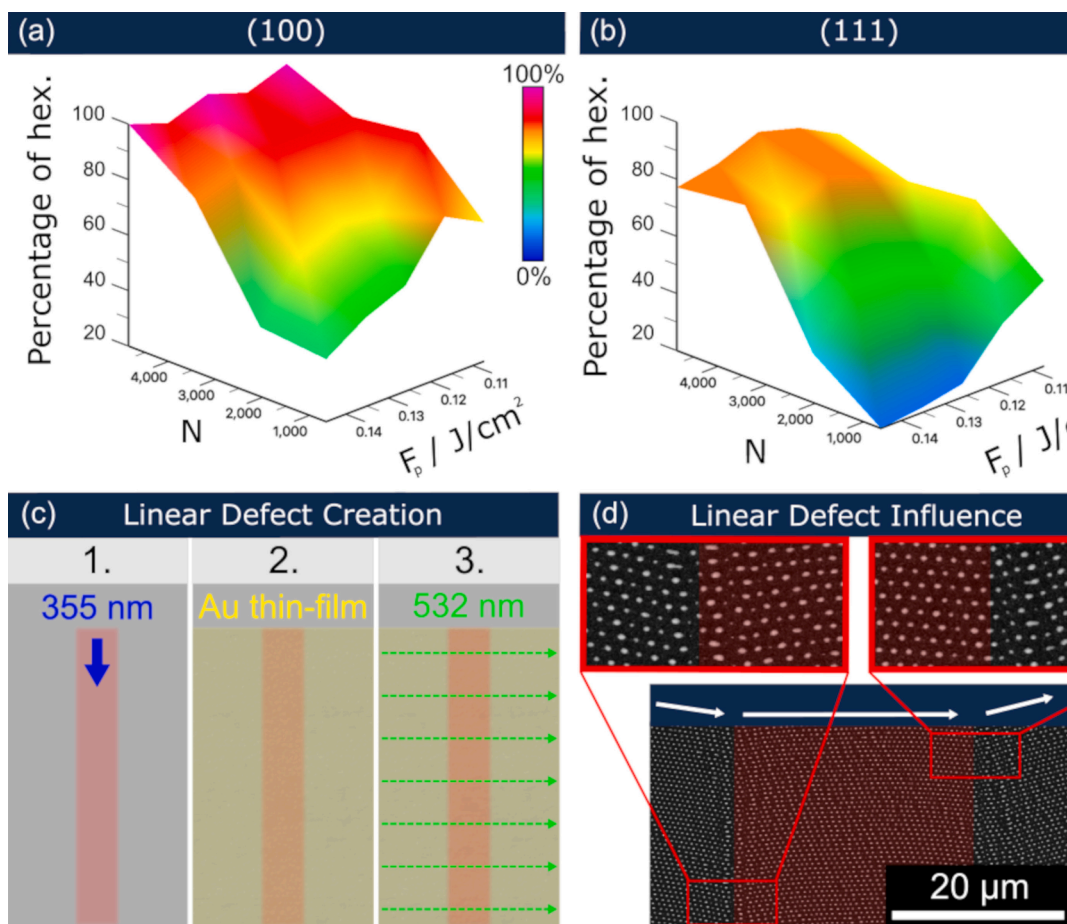
Fig. 8. (a,b) The percentage of hexagonal compared to square structures as a function of effective pulse number N and pulse fluence F_p, for 2D-LIPSS generated on Si (1 0 0)- respectively Si(1 1 1)-substrates. (c) Schematic representation of the linear defect generation. A Si(1 0 0)-Wafer is irradiated with 355 nm ($F_p = 0.127$ J/cm², N = 4, f = 40 kHz) ahead of the usual sample preparation. (d) Deviation of the structure's main axis on an interface of a pre-irradiated (355 nm) and an untreated substrate.
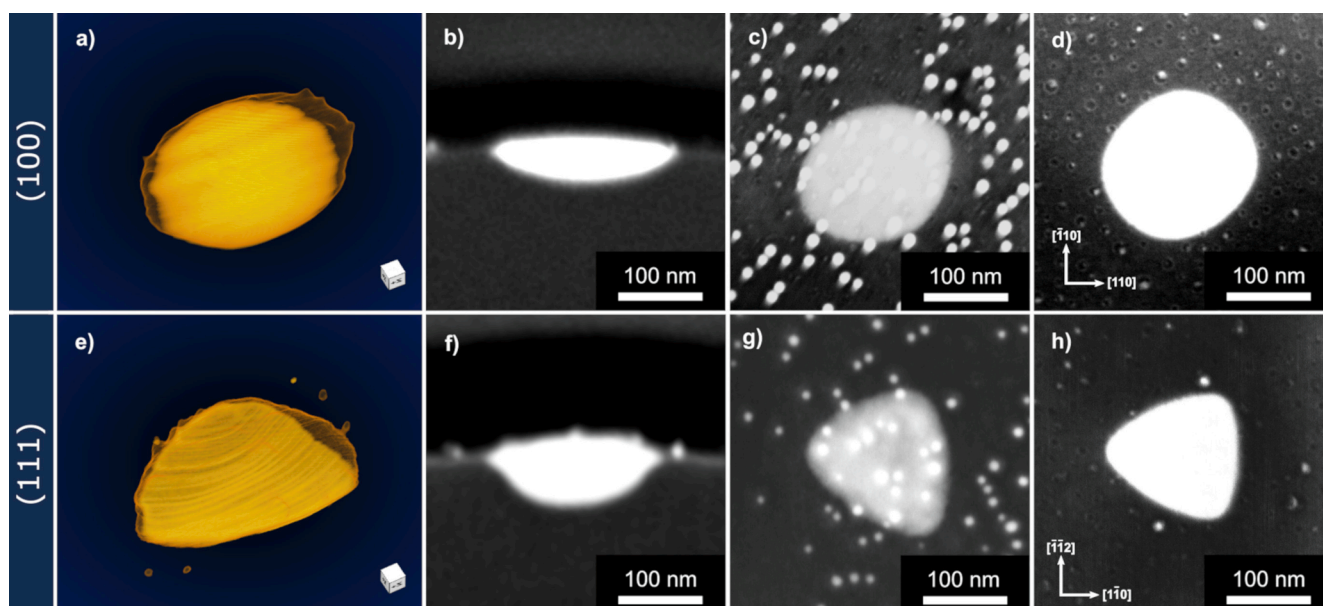

Fig. 9. Morphology of Au nanoparticles generated on Si(1 0 0) (a,b,c,d) and Si(1 1 1) (e,f,g,h) substrates. (a,e) 3D-reconstruction of nanoparticles generated via serial section imaging. (b,f) Cross section of nanoparticles generated by FIB-milling. SEM images of the nanoparticles before (c,g) and after cleaning the surface with aqua regia (d,g).
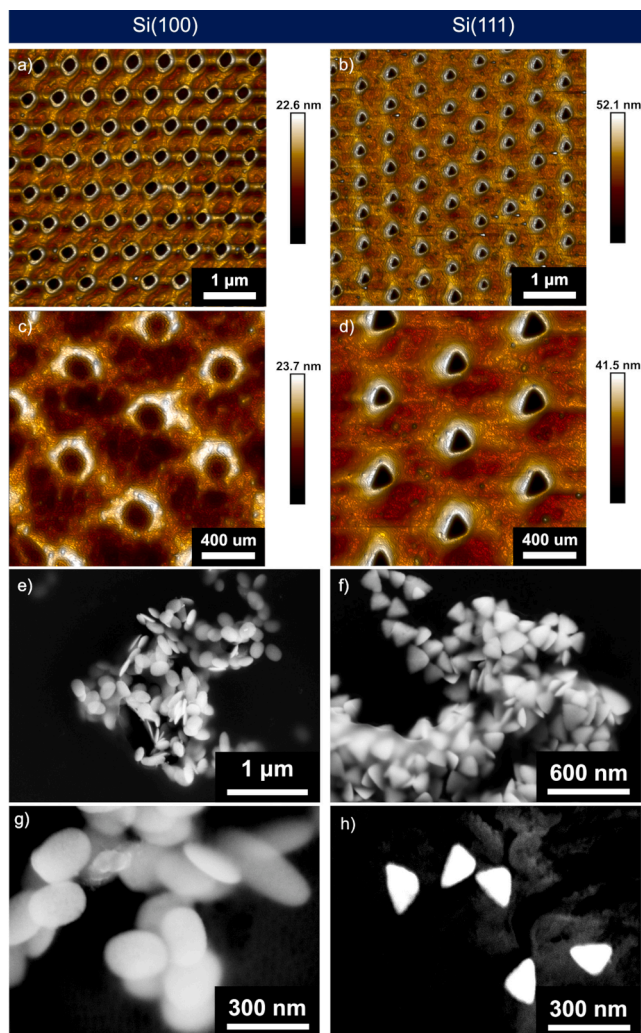
Fig. 10. Nanostructures generated on Si(1 0 0) (a,c,e,g) and Si(1 1 1) (b,d,f,h) substrates. (a,b,c,d) 'Nanohole' array generated in a 2-step etching process with HF and aqua regia. (e,f,g,h) Au nanoparticles after selective destruction of the silicon medium by a 2-step etching process with HF and KOH/2-propanol.

radius of curvature between the particles section above and the section embedded in the silicon wafer (Fig. 9 f). Although kinetics are expected to also play a role in the ns-laser mediated particle formation, the free surface energy of the AuSi-systems interfaces can be qualitatively discussed with equilibrium approaches derived from the Neuman relationship for two melts. As the interface energy-weighted curvatures of

two sides of an embedded particle must be equal, the free energy of the AuSi(1 1 1)- interface $\gamma_{Au,Si(1\,1\,1)}$ is expected to be lower than the corresponding energy of the AuSi(1 0 0) system [55].

Parallel to the surface the nanoparticles fabricated on the Si(1 0 0)-surface are shaped as nearly circular, rounded squares (Fig. 9 c,d), whereas the nanoparticles fabricated on the Si(1 1 1)-surface have the shape of rounded triangles (Fig. 9 g,h). All nanoparticles are facing the exact same orientation which is also dictated by the substrates crystallographic orientation as shown in Fig. 9 (d,h) and can be explained by considering the anisotropy of the substrate's free surface energy. This corresponds to the observations of Ressel et al. [56] for microdroplets of gold on silicon surfaces at different temperatures. The Au droplets were reported to have a triangular equilibrium shape on Si(1 1 1) surfaces and a rounded octagonal shape with 4 dominating faces on Si(1 0 0) surfaces at high temperatures, which are attributed to nucleation effects and Si-surface reconstructions.

Similar to the 1D-LIPSS fabricated by Reinhardt et al. [34], the nanoparticles are surrounded by a thin layer of SiO₂ granting effective protection against acids like nitro-hydrochloric acid (aqua regia) Fig. 9 (d,h). This protective layer is removed by exposing the wafer to hydrofluoric acid (HF, 1 M) for 60 s. Subsequent etching with freshly prepared nitro-hydrochloric acid (aqua regia) leaves behind an array of nano-holes (Fig. 10. a,b,c,d), whereas etching with a boiling mixture of an aqueous solution of potassium hydroxide and isopropanol (4:1) achieves selective destruction of the silicon leaving behind the pristine gold nanoparticles (Fig. 10 e,f,g,h).

The size of the nanoparticles and, therefore also of the holes, is adjustable by varying the gold thin film thickness and the pulse fluency. Generally, a higher film thickness and higher pulse energies increase the particle size (Fig. 11). It exists both an energy and film thickness threshold, whereas an increase of either value does not lead to bigger particles but broader size distributions and arrangement errors. Upon carefully choosing the experimental conditions, the nanoparticles show a very narrow size distribution with a standard deviation of the particle sizes of as low as 1.52 percent, as shown in Appendix A Fig. A3.

4. Conclusion

One-step 2D-nanopatterning of gold thin films on silicon substrates was achieved by circularly polarized ns-laser pulses. By controlling the effective pulse number N, the obtained structures reflect a temporal series of snapshots of the pattern formation, thus representing a suitable tool to study two-dimensional self-organization phenomena. The 2D patterns are obtained as long as there is no dominating orientation of the incident laser light as holds for circular as well as non-polarized light. The evolution of the nanoparticle arrays can be modeled by a feedback-loop of recurring scattered wave interferences. The pattern symmetry can be experimentally controlled by variation of the effective pulse number and fluence to generate extended regions of hexagonal
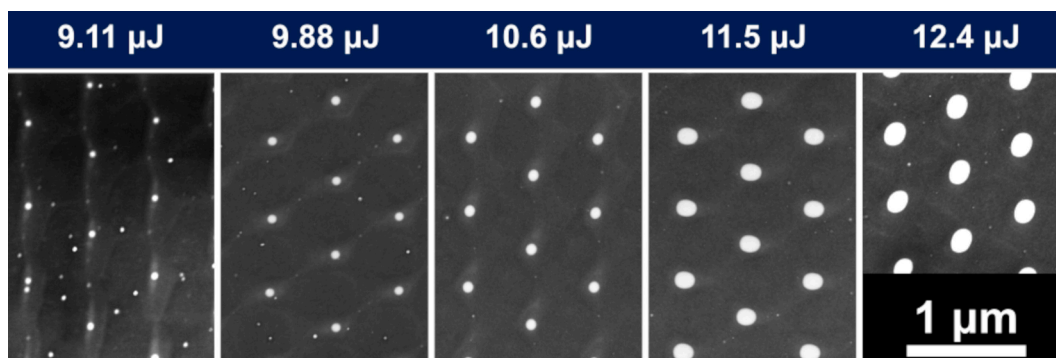

Fig. 11. Adjustment of the size of the nanoparticles upon increasing the pulse energy. (*d* = 1.8 nm, N = *1500*) The samples are rinsed with aqua regia to remove remaining Au leftovers.

nanostructures.

The particle morphology is driven by the substrate's crystallographic orientation and provides lenticular quadrilateral nanoparticles for Si (1 0 0)-substrates and uniformly oriented bulged triangles for Si(1 1 1)-substrates. Different 2-step etching procedures can be used for the fabrication of 'nano-hole' arrays or to harvest the pristine nanoparticles. The size of both the particles and of the holes can be controlled by the film thickness and laser pulse fluence.

The introduced method may be used to study self-organization processes on various two-component systems as well as to serve as a versatile tool for nanoparticle and 'nano-hole' array fabrication or the preparation of small amounts of triangular or quadratic shaped metallic nanoparticles with very narrow size-distributions.

Funding Sources

Declaration of Competing Interest

The authors declare that they have no known competing financial interests or personal relationships that could have appeared to influence the work reported in this paper.

Acknowledgments

Appendix A. Supplementary material

Supplementary data to this article can be found online at https://doi.org/10.1016/j.apsusc.2021.149803.

References

[1] B.K. Nayak, V.V. Iyengar, M.C. Gupta, Efficient light trapping in silicon solar cells by ultrafast-laser-induced self-assembled micro/nano structures, Prog. Photovolt: Res. Appl. 19 (2011) 631–639.

[2] G. Li, J. Li, Y. Hu, C. Zhang, X. Li, J. Chu, W. Huang, Femtosecond laser color marking stainless steel surface with different wavelengths, Appl. Phys. A 118 (2015) 1189–1196.

[3] A.-M. Kietziga, M.N. Mirvakilia, S. Kamalb, P. Englezosa, S.G. Hatzikiriakosa, Nanopatterned metallic surfaces, J. Adhes. Sci. Tech. 25 (2012) 1293–1303.

[4] A.I. Kuznetsov, J. Koch, B.N. Chichkov, Nanostructuring of thin gold films by femtosecond lasers, Appl. Phys. A 94 (2009) 221–230.

[5] A.I. Kuznetsov, A.B. Evlyukhin, M.R. Gonçalves, C. Reinhardt, A. Koroleva, M. L. Arnedillo, R. Kiyan, O. Marti, B.N. Chichkov, Laser fabrication of large-scale nanoparticle arrays for sensing applications, ACS nano 5 (2011) 4843–4849.

[6] F.A. Müller, C. Kunz, S. Gräf, Bio-inspired functional surfaces based on laser-induced periodic surface structures, Materials 9 (2016).

[7] X. Wang, C.J. Summers, Z.L. Wang, Large-scale hexagonal-patterned growth of aligned ZnO nanorods for nano-optoelectronics and nanosensor arrays, Nano Lett. 4 (2004) 423–426.

[8] W. Wang, M. Ramezani, A.I. Väkeväinen, P. Törmä, J.G. Rivas, T.W. Odom, The rich photonic world of plasmonic nanoparticle arrays, Materials Today 21 (2018) 303–314.

[9] Q. Zhou, W. Yang, F. He, R. Stoian, R. Hui, G. Cheng, Femtosecond multi-beam interference lithography based on dynamic wavefront engineering, Opt. Express 21 (2013) 9851–9861.

[10] K.V. Sreekanth, V.M. Murukeshan, Four beams surface plasmon interference nanoscale lithography for patterning of two-dimensional periodic features, J. Vac. Sci. Technol 28 (2010) 128–130.

[11] H.M. Reinhardt, P. Maier, H.-C. Kim, D. Rhinow, N. Hampp, Nanostructured transparent conductive electrodes for applications in harsh environments fabricated via nanosecond laser-induced periodic surface structures (LIPSS) in indium-tin oxide films on glass, Adv. Mater. Interfaces 30 (2019) 1900401.

[12] M. Birnbaum, Semiconductor surface damage produced by Ruby lasers, J. Appl. Phys. 36 (1965) 3688–3689.

[13] O. Varlamova, F. Costache, J. Reif, M. Bestehorn, Self-organized pattern formation upon femtosecond laser ablation by circularly polarized light, Appl. Surf. Sci. 252 (2006) 4702–4706.

[14] J. Bonse, A. Rosenfeld, J. Krueger, SPPOnSurfaceDefect_Bonse2009, J. Appl. Phys. 106 (2009) 104910.

[15] F. Garrelie, J.P. Colombier, F. Pigeon, S. Tonchev, N. Faure, M. Bounhalli, S. Reynaud, O. Parriaux, Evidence of surface plasmon resonance in ultrafast laser-induced ripples, Opt. Express 19 (2011) 9035–9043.

[16] T.J.-Y. Derrien, T.E. Itina, R. Torres, T. Sarnet, M. Sentis, Possible surface plasmon polariton excitation under femtosecond laser irradiation of silicon, J. Appl. Phys. 114 (2013) 83104.

[17] H.M. Reinhardt, K. Bücker, N.A. Hampp, Directed assembly of gold nanowires on silicon via reorganization and simultaneous fusion of randomly distributed gold nanoparticles, Opt. express 23 (2015) 11965–11974.

[18] P. Nürnberger, H. Reinhardt, H.-C. Kim, F. Yang, K. Peppler, J. Janek, N. Hampp, Influence of substrate microcrystallinity on the orientation of laser-induced periodic surface structures, J. Appl. Phys. 118 (2015) 134306.

[19] I. Gnilitskyi, T.J.-Y. Derrien, Y. Levy, N.M. Bulgakova, T. Mocek, L. Orazi, High-speed manufacturing of highly regular femtosecond laser-induced periodic surface structures, Sci. Rep. 7 (2017) 8485.

[20] P. Nürnberger, H.M. Reinhardt, H.-C. Kim, E. Pfeifer, M. Kroll, S. Müller, F. Yang, N.A. Hampp, Orthogonal superimposed laser-induced periodic surface structures (LIPSS) upon nanosecond laser pulse irradiation of SiO 2 /Si layered systems, Appl. Surf. Sci. 425 (2017) 682–688.

[21] J. Bischof, D. Scherer, S. Herminghaus, P. Leiderer, Dewetting modes of thin metallic films: nucleation of holes and spinodal dewetting, J. Appl. Phys. 106 (2009) 104910.

[22] G.D. Tsibidis, C. Fotakis, E. Stratakis, From ripples to spikes, Phys. Rev. B 92 (2015) 041405.

[23] J.Z.P. Skolski, G.R.B.E. Römer, J.V. Obona, V. Ocelik, A.J. Huis in 't Veld, J.T.M. de Hosson, Laser-induced periodic surface structures: Fingerprints of light localization, Phys. Rev. B 85 (2012) 075320.

[24] G. Deng, G. Feng, S. Zhou, Experimental and FDTD study of silicon surface morphology induced by femtosecond laser irradiation at a high substrate temperature, Opt. Express 25 (2017) 7818–7827.

[25] M.C. Cross, P.C. Hohenberg, Pattern formation outside of equilibrium, Rev. Modern Phys. (1993) 851–1086.

[26] G.D. Tsibidis, M. Barberoglou, P.A. Loukakos, E. Stratakis, C. Fotakis, Dynamics of ripple formation on silicon surfaces by ultrashort laser pulses in subablation conditions, Phys. Rev. B 86 (2012) 013901.

[27] R. Wehner, R. Grunwald, Feedback-driven plasmonic-thermal route to femtosecond-laser-induced periodic surface structures in silicon indicated by pump-probe scattering and diffraction, Surfaces 2 (2019) 277–294.

[28] F. Fraggelakis, G. Mincuzzi, J. Lopez, I. Manek-Hönninger, R. Kling, Controlling 2D laser nano structuring over large area with double femtosecond pulses, Appl. Surf. Sci. 470 (2019) 677–686.

[29] G. Giannuzzi, C. Gaudiuso, R. Di Mundo, L. Mirenghi, F. Fraggelakis, R. Kling, P. M. Lugarà, A. Ancona, Short and long term surface chemistry and wetting behaviour of stainless steel with 1D and 2D periodic structures induced by bursts of femtosecond laser pulses, Appl. Surf. Sci. 494 (2019) 1055–1065.

[30] Q. Liu, N. Zhang, J. Yang, H. Qiao, C. Guo, Direct fabricating large-area nanotriangle structure arrays on tungsten surface by nonlinear lithography of two femtosecond laser beams, Opt. Express 26 (2018) 11718–11727.

[31] A. Abou Saleh, A. Rudenko, S. Reynaud, F. Pigeon, F. Garrelie, J.-P. Colombier, Sub-100 nm 2D nanopatterning on a large scale by ultrafast laser energy regulation, Nanoscale 12 (2020) 6609–6616.

[32] S. van der Poel, M. Mezera, G.-W. Römer, E. de Vries, D. Matthews, Fabricating laser-induced periodic surface structures on medical grade cobalt–chrome–molybdenum, Lubricants 7 (2019) 70.

[33] J.-M. Romano, A. Garcia-Giron, P. Penchev, S. Dimov, Triangular laser-induced submicron textures for functionalising stainless steel surfaces, Appl. Surf. Sci. 440 (2018) 162–169.

[34] H. Reinhardt, K. Bücker, F. Yang, P. Nürnberger, N.A. Hampp, Highly dynamic alloying and dealloying in the model system gold-silicon (AuSi), J. Phys. Chem. C 119 (2015) 5462–5466.

[35] L.W. Barnes, A. Dereux, T.W. Ebbesen, Surface plasmon subwavelength optics, Nature 424 (2003) 824–830.

[36] M. Huang, F. Zhao, Y. Cheng, N. Xu, Z. Xu, Origin of laser-induced near-subwavelength ripples, ACS nano 3 (2009) 4062–4070.

[37] P.E. Ciddor, Refractive index of air: new equations for the visible and near infrared, Appl. Opt. 35 (1996) 1566–1573.

[38] G.E. Jellison, D.H. Lowndes, Measurements of the optical properties of liquid silicon and germanium using nanosecond time-resolved ellipsometry, Appl. Phys. Lett. 51 (1987) 352–354.

[39] Y. Kaganovskii, H. Vladomirsky, M. Rosenbluh, Periodic lines and holes produced in thin Au films by pulsed laser irradiation, J. Appl. Phys. 100 (2006) 44317.

[40] C.V. Thompson, Solid-state dewetting of thin films, Annu. Rev. Mater. Res. 42 (2012) 399–434.

[41] L. Kondic, A.G. González, J.A. Diez, J.D. Fowlkes, P. Rack, Liquid-state dewetting of pulsed-laser-heated nanoscale metal films and other geometries, Annu. Rev. Fluid Mech. 52 (2020) 235–262.

[42] F. Brochard Wyart, J. Daillant, Drying of solids wetted by thin liquid films, Can. J. Phys. 68 (1990) 1084–1088.

[43] C. Favazza, R. Kalyanaraman, R. Sureshkumar, Robust nanopatterning by laser-induced dewetting of metal nanofilms, Nanotechnology 17 (2006) 4229–4234.

[44] R.V. Craster, O.K. Matar, Dynamics and stability of thin liquid films, Rev. Mod. Phys. 81 (2009) 1131–1198.

[45] E.L. Gurevich, Self-organized nanopatterns in thin layers of superheated liquid metals, Phys. Rev. E 83 (2011) 31604.

[46] J.E. Sipe, Jeff F. Young, J.S. Preston, H.M. van Driel, Laser-induced periodic surface structure. I. Theory Phys. Rev. B 27 (1983) 1141-1154.

[47] H.M. van Driel, J.E. Sipe, J.F. Young, Laser-induced periodic surface structure on solids: a universal phenomenon, Phys. Rev. Lett. 49 (1982) 1955–1959.

[48] B. Öktem, I. Pavlov, S. Ilday, H. Kalaycıoğlu, A. Rybak, S. Yavaş, M. Erdoğan, F.Ö. Ilday, Nonlinear laser lithography for indefinitely large-area nanostructuring with femtosecond pulses, Nat. Photonics 7 (2013) 897–901.

[49] A. Gailtis, Formation of the hexagonal pattern on the surface of a ferromagnetic fluid in an applied magnetic field, J. Fluid Mech. 82 (1977) 401–413.

[50] C. Kubstrup, H. Herrero, C. Perez-Garcia, Fronts between hexagons and squares in a generalized Swift-Hohenberg equation, Phys. Rev. E 54 (1996) 1560–1569.

[51] A. Thess, S.A. Orszag, Temperature spectrum in surface tension driven Bénard convection, Phys. Rev. Lett. 73 (1994) 541–555.

[52] M.F. Schatz, S.J. VanHook, W.D. McCormick, J.B. Swift, H.L. Swinney, Time-independent square patterns in surface-tension-driven Bénard convection, Phys. Fluids 11 (1999) 2577–2582.

[53] N. Casquero, Y. Fuentes-Edfuf, R. Zazo, J. Solis, J. Siegel, Generation, control and erasure of dual LIPSS in germanium with fs and ns laser pulses, J. Phys. D: Appl. Phys. 53 (2020) 485106.

[54] E.J. Siem, W.C. Carter, D. Chatain, The equilibrium shape of anisotropic interfacial particles, Philos. Mag. Lett. 84 (2004) 991–1010.

[55] W.D. Kaplan, D. Chatain, P. Wynblatt, W.C. Carter, A review of wetting versus adsorption, complexions, and related phenomena, J Mater Sci 48 (2013) 5681–5717.

[56] B. Ressel, K.C. Prince, S. Heun, Y. Homma, Wetting of Si surfaces by Au–Si liquid alloys, J. Appl. Phys. 93 (2003) 3886–3892.